Canadian Science Publishing
NRC Research Press journals | Publishing Services

Biochemistry and Cell Biology
Biochimie et biologie cellulaire

MAHOGUNIN MEDIATED REGULATION OF $G\alpha_i$ LOCALISATION DURING MITOSIS AND ITS EFFECT ON SPINDLE POSITIONING

Journal:	*Biochemistry and Cell Biology*
Manuscript ID	bcb-2015-0161.R1
Manuscript Type:	Note
Date Submitted by the Author:	31-Mar-2016
Complete List of Authors:	Srivastava, Devika; Saha Institute of Nuclear Physics, Biophysics & Structural Genomics Mukherjee, Rukmini ; Saha Institute of Nuclear Physics, Biophysics and Structural Genomics Mookherjee, Debdatto; Saha Institute of Nuclear Physics, Biophysics and Structural Genomics Chakrabarti, Oishee; Saha Institute of Nuclear Physics, Biophysics and Structural Genomics
Keyword:	MGRN1, Gαi, spindle positioning defects, ternary complex, cortical enrichment

MAHOGUNIN MEDIATED REGULATION OF Gα$_i$ LOCALISATION DURING MITOSIS AND ITS EFFECT ON SPINDLE POSITIONING

Devika Srivastava#, Rukmini Mukherjee, Debdatto Mookherjee and Oishee Chakrabarti*

Biophysics & Structural Genomics Division, Saha Institute of Nuclear Physics, 1/AF Bidhannagar, Kolkata – 700064, India

*Correspondence: oishee.chakrabarti@saha.ac.in

Co-corresponding author: devika.srivastava@saha.ac.in

ABBREVIATIONs

Ar, Argon; a.u., arbitrary units; G2/M, Gap2/Mitotic Phase; GDP, Guanosine-5'-diphosphate; GFP, Green Fluorescent Protein; GPCR, G-Protein-Coupled Receptors; GTP, Guanosine-5'-triphosphate; HA, Hemagglutinin; He-Ne, Helium-Neon; IgG, Immunoglobulin G; LGN, Leucine-Glycine-Asparagine (mammalian homologue of Pins); MCR, Melanocortin Receptor; MGRN1, Mahogunin Ring Finger1; MTs, Microtubules; Mud, Mushroom Body Defect; NA, Numerical Aperture; NEBD, Nuclear Envelope Breakdown; *nes*, Nuclear Exit Signal; *nls*, Nuclear Localisation Signal; Noc, Nocodazole; NuMa, Nuclear Mitotic Apparatus; PBS, Phosphate Buffer Saline; Pins, Partner of Inscuteable; PSAP,Proline-Serine-Alanine-Proline; qRT-PCR, quantitative reverse transcription polymerase chain reaction; RFP, Red Fluorescent Protein; RING, Really Interesting New Gene; TSG101, Tumor Suppressor Gene 101; Ub, Ubiquitin; YFP, Yellow Fluorescent Protein.

Key words: MGRN1, Gα$_i$, spindle positioning defects, ternary complex, cortical enrichment

Running Title: MGRN1 regulates Gα$_i$ to orient spindles

ABSTRACT

Mahogunin RING Finger 1 (MGRN1) is a ubiquitin E3 ligase known to affect spindle tilt in mitotic cells by regulating α-tubulin ubiquitination and polymerization. In cell culture systems we have found that expressing truncated mutants of MGRN1 lead to various other mitotic anomalies, like lateral and angular spindle displacements. This seems independent of the MGRN1 ligase activity. Our experiments suggest that MGRN1 regulates the balance between the lower molecular weight monomeric Gα$_i$ and larger trimeric G-protein complex, along with its abundance in the ternary complex that regulates spindle positioning. The cytosolic isoforms of MGRN1 lead to the enrichment of monomeric Gα$_i$ in the cytosol and its subsequent recruitment at the plasma membrane. Excess Gα$_i$ at the cell cortex results in an imbalance in the assembly of the ternary complex regulating spindle positioning during mitosis. These observations seem independent of the ligase activity of MGRN1 though we cannot negate the involvement of an intermediate player which acts as a substrate for MGRN1 and in turn, regulates Gα$_i$.

INTRODUCTION

In all organisms cell division is a finely co-ordinated ensemble of events, essential for maintaining the integrity of genetic information transmitted to daughter cells. A key factor that governs cell division in eukaryotes is the integrity, positioning and orientation of the mitotic spindle – referred henceforth as "spindle positioning" (Kotak et al. 2012). This essentially guides the spindle apparatus towards asymmetric division in stem cells and gives rise to cells of different lineages or dictates the relative size of daughter cells (Gillies and Cabernard 2011; Morin and Bellaiche 2011; Srivastava and Chakrabarti 2015). Accurate spindle positioning is crucial for equal distribution of cellular constituents and generation of identical cells in symmetric cell division (Gonczy 2008; Gillies and Cabernard 2011; Morin and Bellaiche 2011).

The proteins at the core of the machinery that regulate spindle positioning are known to be evolutionarily conserved across species. The orientation of mitotic spindle is regulated via pulling forces exerted on the astral microtubules (MTs) by Dynein/Dynactin complexes recruited at the cell cortex by a conserved ternary protein complex. In mammalian systems, this consists of a member of heterotrimeric G-protein complex, Gα$_i$ which is recruited at the plasma membrane via its myristoylation domain. Membrane associated Gα$_i$ in turn engages with LGN and NuMA to form the complex at the membrane (Du and Macara 2004). The role of Gα$_i$ as a crucial regulator of the spindle positioning machinery is independent of its canonical role in cell signalling pathways. It is noteworthy that the monomeric Gα$_i$– GDP, dissociated from the G$_{\beta\gamma}$ is recruited to the membrane and not the active GTP bound form of the protein (Woodard et al. 2010). This tripartite complex then recruits Dynein to the membrane.There it exerts the forces necessary for regulation of spindle positioning (Du and Macara 2004). Various analogs of this complex have been identified in other organisms -- Gα/GPR-1/2/Lin-5 in worms and Gα-Pins-Mud in flies (Bird et al. 2013; Gonczy 2008; McNally 2013; Siller and Doe 2009; Stevermann and Liakopoulos 2012).

The key regulators of spindle positioning are well identified. The molecular mechanisms guiding these players to their destination are, however, still progressively being explored.

Studies in various cell lines have shown that a higher concentration of Gα$_i$ at the membrane corresponds with an increase in the levels of LGN and NuMA at the cortex (Du and Macara 2004; Kotak et al. 2012). Overexpression of the ternary complex components (Gα$_i$ or LGN) leads to enrichment of p150Glued at the cortical membrane and also overall

enhanced levels of this Dynactin subunit in cells (Kotak et al. 2012). It is also reported that higher concentration of the tripartite complex at the membrane leads to dramatic spindle oscillations in metaphase spindle (Du and Macara 2004; Kotak et al. 2012; Matsumura et al. 2012), detrimental to its correct positioning.

In this study we have shown that the cytosolic E3 ubiquitin ligase, MGRN1 (Mahogunin RING Finger 1) is an important modulator of Gα$_i$, affecting the recruitment of this component of the ternary complex to the membrane during mitosis. This function of MGRN1 seems independent of its ligase activity. Previous report from our laboratory has elucidated that MGRN1 regulates microtubule polymerization and affects spindle tilt in cell culture systems (Srivastava and Chakrabarti 2014). MGRN1 has been shown to compete with and displace Gα$_s$ for its binding to melanocortin receptor (MC1R and MC4R, a GPCR) in cell lines. This alleviates signalling events downstream of the GPCR. Here MGRN1 functions independent of its ligase activity. Its various isoforms and splice variants might have different functions based on their differential distribution in multiple cellular compartments (Jiao et al. 2009; Perez-Oliva et al. 2009). Our present study attributes another function to MGRN1 where it modulates spindle positioning by stabilizing the Gα$_i$-GDP at the cortex in mitotic cells.

MATERIALS AND METHODS

Constructs, antibodies and reagents

MGRN1, MGRN1ΔR, MGRN1ΔN, MGRN1ΔC, and C316DMGRN1 constructs have been described before (Srivastava and Chakrabarti 2014). SRAP MGRN1-GFP has been described previously (Majumder and Chakrabarti 2015). MGRN1I201D-RFP was generated using standard site directed mutagenesis protocol. MGRN1ΔN150-RFP and MGRN1ΔN200-RFP were generated using standard cloning techniques. HA-tagged wild-type Ub was a gift of Rafael Mattera (Bethesda, MD, USA).

Antibodies were from the following sources: α-tubulin (Santa Cruz Biotechnology), γ-tubulin (Sigma), Dynein (Thermo Scientific™ Pierce), NuMa (Abcam) and Gα$_i$ (Abcam). MGRN1, GFP, RFP and HA antibodies were gifts of Ramanujan S Hegde (Cambridge, UK).

MG132 (Sigma-Aldrich) was used at 100μM concentration for 45 minutes; 5mM thymidine (Sigma-Aldrich) for 16-18 hours; 100ng/ml nocodazole (Sigma-Aldrich) block for 16 hours.

Cell culture, synchronization and immunocytochemistry

Cell line used for the experiment was HeLa (human cervical cancer cell line).Cells were cultured, transfected, immunostained and imaged as before (Chakrabarti and Srivastava 2014). All tissue culture plasticware and Lab-Tek 8-well chambered slides used for microscopy were from Nunc, Rosklide, Denmark, and bottom coverglass dishes used for microscopy were from SPL Lifesciences, Gyeonggi-do, Korea. Cell were synchronized by thymidine–nocodazole treatment as described previously (Srivastava and Chakrabarti 2014). For MG132 proteasomal blocking assay, HeLa cells were first mitotically enriched. After the removal of nocodazole, cells were treated with MG132, following which they were lysed using Lameli buffer.

Western blotting and immunoprecipitation

The protocol for western blotting was as before (Srivastava and Chakrabarti 2014). For native PAGE, cells were lysed under non-denaturing conditions, using mechanical disruption. Briefly, the cells were lysed in detergent free lysis buffer (50 mM Tris HCl pH 7.5, 25mM NaCl, 1 mM EDTA,1mM PMSF, 0.1% Triton-X), followed by breakage of cells by syringe lysis. The samples were made in 5X native loading dye (1m Tris pH 6.8, 100% glycerol, Bromophenol blue, 500 mM Aminocaproic Acid) without boiling, followed by resolution of the proteins in an SDS- free 10% tris-glycine gel.

Fluorescence microscopy and imaging

Fluorescence microscopy was performed utilizing LSM510-Meta, LSM710/ConfoCor 3 microscopy systems (Zeiss, Jena, Germany) or Nikon N-SIM Super-Resolution Microscope equipped with an Ar-ion laser (for GFP excitation or Alexa-Flour 488 with the 488 nm line), a helium–neon (He-Ne) laser (for RFP, Alexa-Fluor 546 and 594 excitation with the 543 line) and a He-Ne laser (for Alexa- Fluor 633 with the 633 line). For all imaging on LSM510 or LSM 710, 63X1.4 numerical aperture (NA) oil immersion objective was used while for Nikon N-SIM Super-Resolution Microscope, 100X1.4 numerical aperture (NA) oil immersion objective was used.

Image analyses and calculation of spindle tilt

ImageJ (NIH, Bethesda, MD, USA) was used for all the image analyses reported. For calculation of tilt in cells, z-stack images were taken with a z-spacing of 0.5–1.0 μm and

normalized as required. The distance between the poles was estimated by using ImageJ and then the spindle tilt was calculated as described before (Srivastava and Chakrabarti 2014). The intensity was calculated using ImageJ. For analysis of the cortical distribution of members of ternary complex, a straight line was drawn across the longitudinal axis of the cell, and the intensity distribution along this axis was quantitated using ImageJ. The intensity distribution for all the cells in the sample set was taken using ImageJ and the mean for each point along the longitudinal axis was quantitated using Microsoft Excel. Lateral displacement studies were done as described before (Kiyomitsu and Cheeseman 2012). For angular displacement studies, the angle between the longitudinal axis of the cell and the spindle axis (perpendicular to the chromosomal plate) was determined. The mean of all such angles was considered as the angular displacement of the sample set.

Nuclear Fractionation

HeLa cells from a confluent 60mm dish transiently transfected with RFP tagged MGRN1 or its truncated mutants were lysed in 300µl of hypotonic buffer [10mM Hepes (pH=7.4), 2mM $MgCl_2$, 25mM KCl,1mM DTT,1mM PMSF, protease inhibitor cocktail]. Cells were kept on ice for 30min followed by syringe lysis. 125µl of 2M sucrose solution was added dropwise, followed by centrifugation at 1000rpm for 15min.The supernatant was saved as the cytosolic fraction. The pellet waswashed twice in wash buffer [10mM Hepes (pH=7.4), 2mM $MgCl_2$, 25mM KCl, 250mM sucrose, 1mM DTT, 1mM PMSF, protease inhibitor cocktail] and saved as the nuclear fraction.

Real Time PCR

Cells were co-transfected with MGRN1 or its truncated mutants and Gα$_i$-YFP. Total RNA was extracted from HeLa cells using Trizol reagent (Invitrogen, USA) and subsequently treated with RNAse free-DNAse (Roche) and quality assayed (Nanodrop 2000c, Thermo Scientific). The cDNA was prepared by reverse transcribing 1000ng of total RNA with reverse transcriptase reagents (Thermo Scientific RevertAid Reverse Transcriptase). Quantitative PCR was subsequently performed using SYBR Green core PCR reagents (Applied Biosystems) and primers against GAPDH and GFP. The qRT–PCR reactions and analyses were carried out in 7500 Sequence Detection System (Applied Biosystems). ΔCt values were calculated from Ct values of GAPDH and GFP. Details of the primer sequences (5'→ 3') are as follows:

GAPDH Fwd: AGAAGGCTGGGGCTCATTTG
GAPDH Rev: AGGGGCCATCCACAGTCTTC
GFP Fwd: AAGCTGACCCTGAAGTTCATCTGC
GFP Rev: CTTGTTGCCGTCGTCCTTGAA

RESULTS

Catalytic inactivation of MGRN1 alters spindle positioning

It has been previously reported that MGRN1 regulates spindle tilt in various cell culture systems (Srivastava and Chakrabarti 2014). Presence of MGRN1 mutants leads to increase in the spindle angle relative to the cell-substrate adhesion plane, significantly more than the control cells expressing the functional ligase (Fig. S1 A, B, C, D). In addition to aberrations in spindle tilt (along z-axis), presence of these MGRN1 mutants (lacking the RING domain, referred to as MGRN1ΔR or the C-terminus, namely MGRN1ΔC) result in other mitotic defects like lateral and angular displacements of the spindle apparatus (in the *xy* plane) (Fig.1A). Like MGRN1ΔR, cells transiently expressing MGRN1ΔC fail to ubiquitinate α-tubulin (Fig. S1E). Significant lateral spindle displacement was observed in the *xy* plane in cells expressing MGRN1ΔR (~1.4 folds) (Fig. 1B, C, D) or MGRN1ΔC (~1.3 folds) (Fig. 1F, G, H) in comparison with control cells. Similarly, increase in the angular spindle displacement from long axis of the cell was observed in the presence of MGRN1ΔR (~1.4 folds) or MGRN1ΔC (~1.3 folds) when compared with their respective controls (Fig. 1E, I). Since defects in lateral and angular displacements were abundant in cells with MGRN1 truncated mutants, it was obvious to assess if factors other than integrity of MTs governed the displacement of the mitotic spindles.

Functionally inactive MGRN1 perturbs localisation of the ternary complex components of spindle positioning

Localisation of the Dynein motor protein along with the components of the ternary complex (LGN, NuMA and Gα$_i$) that guide spindle positioning was evaluated. Dynein exerts the force necessary to position the spindle apparatus in the centre of the cell (Kotak et al. 2012). High amounts of dynein are present at the poles during mitosis (Fig. S2A, B). In MGRN1-RFP over-expressing cells too, elevated levels of Dynein was detected at the mitotic poles, in comparison with the rest of the cell (Fig. S2C, D). However, high resolution z-projection images indicated that low amounts of Dynein was detected at the poles in cells expressing MGRN1ΔR-RFP. Alternately we can state that MGRN1ΔR-RFP expressing cells had higher amounts of Dynein at the membrane than at the poles in comparison to control cells. While with functional MGRN1-RFP, the dynein expression ratio at the pole: cortex was ~ 0.7, in the presence of MGRN1ΔR-RFP this ratio was ~1.4 (Fig. S2E).

Similarly, Gα$_i$ and NuMA were more abundant at the cortex in MGRN1ΔR-RFP or MGRN1ΔC-RFP expressing cells, compared to those with MGRN1-RFP (Fig. 2, S2F, G). LGN also showed a skewed pattern of protein distribution in mitotic MGRNΔ1R cells (*data not shown*). Like Dynein, the pole:cortex ratio of NuMA protein distribution was higher in MGRN1-RFP control cells versus those with MGRN1ΔR-RFP (Fig. S2H). Similarly, the cortical localization of Gα$_i$ was also studied in mitotic cells using a fluorescently tagged construct (Fig. 2A, B). Elevated levels of Gα$_i$-YFP were detected at cortex of cells expressing MGRN1ΔR-RFP or MGRN1ΔC-RFP, co-transfected with Gα$_i$-YFP (Fig. 2C-E). Results so far suggested that lateral and angular displacements observed with catalytic inactivation of MGRN1 were probably due to altered localization of the ternary complex proteins responsible for mitotic spindle positioning.

MGRN1 modulates Gα$_i$ levels

It is reported that overexpression of one of the components of the ternary complex leads to enrichment of some of the other molecular players responsible for spindle positioning at the cortical membrane (Kotak et al. 2012), possibly independent of spindle integrity. Hence we checked for the expression levels of Dynein, NuMA and Gα$_i$ in mitotically enriched cell lysates. The protein levels of Dynein and NuMA were similar in cells expressing either MGRN1-RFP or its variants (Fig. 3A). However, increase in endogenous Gα$_i$ protein levels was detected in MGRN1ΔR-RFP and MGRN1ΔC-RFP cell lysates as compared with MGRN1-RFP or another mutant lacking the N-terminus (MGRN1ΔN-RFP). Significant increase was also seen when Gα$_i$-YFP was overexpressed in cells, along with truncated mutants of MGRN1 (Fig. 3A, B). Post-translational lipid modifications, like myristoylation, palmitoylation and prenylation of the heterotrimeric G-protein subunits help in their membrane targeting and anchorage (Chen and Manning 2001). It has been previously shown that a mutant of Gα$_i$ that cannot be myristoylated or palmitoylated (Gα$_i$-Δmyr) acts as a competitive inhibitor of the endogenous protein (Kotak et al. 2012). This mutant does not localise to the plasma membrane, in turn compromising the amounts of p150Glued at the cell cortex. We found that increase in levels of Gα$_i$ was independent of its myristoylation domain since expression of Gα$_i$Δmyr-YFP also led to elevated levels of Gα$_i$ in the presence of MGRN1ΔR and MGRN1ΔC, compared to MGRN1 (Fig. S3A, B). This suggested that the Gα$_i$ levels were regulated by MGRN1 directly or indirectly, whereby its functionally inactive form stabilised Gα$_i$ at the cell cortex. Interestingly, overexpression of point mutants of

MGRN1 with changes in the RING domain (C316D MGRN1-GFP) or the PSAP motif (responsible for interaction with TSG101, referred to as SRAP MGRN1-GFP) did not have any effect on the expression levels of Gα$_i$-YFP in the cell (Fig. S3C).

MGRN1 does not regulate Gα$_i$ at the translational or transcriptional levels

Since MGRN1 is an E3 ubiquitin ligase known to ubiquitinate multiple substrates (Kim et al. 2007; Srivastava and Chakrabarti 2014), we checked whether Gα$_i$ was ubiquitinated and degraded in the presence of MGRN1. Similar expression pattern of Gα$_i$-YFP was detected with or without the drug treatment across all samples co-transfected with MGRN1-RFP or its truncated mutants (Fig. 3C). β-catenin was however seen to accumulate with MG132 treatment across samples, indicating that the drug could effectively block proteasome. Similar expression pattern of Gα$_i$-YFP between MG132 treated and untreated samples suggested that MGRN1 was not involved in modulating the turnover of this protein. This, however, did not completely rule out the possibility that MGRN1 could still ubiquitinate Gα$_i$; this modification need not lead to protein degradation. In an *in vivo* ubiquitination assay, lysates derived from HeLa cells co-transfected with MGRN1-RFP, MGRN1ΔR-RFP or MGRN1ΔC-RFP and HA-Ub and Gα$_i$-YFP, were immunoprecipitated against Gα$_i$-YFP and immunoblotted for exogenously expressed ubiquitin (Fig. 3D, lanes [ii-iv]). No poly-ubiquitination ladder was detected in any of the samples. To authenticate the efficiency of this experiment, ubiquitination of α–tubulin was verified in a similar assay (Fig. 3D, lane [i]). Detection of strong signal for polyubiquitined species of α–tubulin confirmed that both MGRN1 and HA-tagged ubiquitin were functional. Hence implicating that MGRN1 does not potentiate ubiquitination and degradation of Gα$_i$.

We next checked if MGRN1 was modulating Gα$_i$ at the transcription level. MGRN1 is primarily a cytosolic protein which has four isoforms in the cell. While all the splice variants of MGRN1 contain *nes* (Nuclear Exit signal), two of its isoforms also additionally contain *nls* (Nuclear Localization Signal) (Fig 3E) (Jiao et al. 2009). This indicates that a fraction of the cellular pool of MGRN1 is targeted to the nucleus, where it possibly performs additional functions, distinct from its cytoplasmic counterparts. One possible function could be alteration of Gα$_i$ transcription, to justify its elevated protein levels. RNA was isolated from mitotic cells co-transfected with Gα$_i$-YFP and empty vector RFP, MGRN1-RFP or its truncated mutants (MGRN1ΔR-RFP or MGRN1ΔC-RFP). Real time qRT PCR analysis

showed no significant change in the transcripts levels of Gα$_i$-YFP across the samples (Fig. 3F).

Non-canonical modulation of Gα$_i$ by MGRN1

Since the data indicated clearly that MGRN1 did not alter Gα$_i$ translationally, post-translationally or even transcriptionally, it suggested the possibility of a non-canonical function for the E3 ligase. As indicated earlier, Gα$_i$-GDP dissociated from the G-protein complex is recruited to the membrane. Hence, we argued if there was a correlation between the steady-state levels of the monomeric protein and expression of MGRN1 or its truncated mutants. The steady-state level of the monomeric protein was higher in presence of MGRN1ΔR-RFP or MGRN1ΔC-RFP than MGRN1-RFP. On a native PAGE, enrichment of a lower molecular weight monomeric Gα$_i$-YFP and corresponding lesser abundance of the trimeric G-protein complex was detected in cells expressing Gα$_i$-YFP and MGRN1ΔR-RFP or MGRN1ΔC-RFP than in the presence of MGRN1-RFP (Fig. 4A, B).

Careful examination of the sequence of the four isoforms of MGRN1 showed presence of *nls* (amino acids 359-375) downstream of the RING domain of the protein, in its C-terminal. Truncation of MGRN1 between (amino acids 252-325) to generate MGRN1ΔR probably compromised its *nls* while MGRN1ΔC (amino acids 308-533) totally lacked this motif (Fig. S1D, Fig. 3E). We hypothesised that overexpression of truncated mutants skewed the internal balance between the cellular levels of the isoforms of MGRN1. Cell fractionation studies showed that while MGRN1-RFP was primarily cytosolic, a small fraction of it was detected in nuclear extracts. This sub-cellular partitioning of MGRN1, however, changed in the presence of MGRN1ΔR-RFP where a decline was seen in the nuclear fraction. MGRN1 was almost entirely detected in the cytosolic fraction in the presence of MGRN1ΔC-RFP (Fig.4C-F). However, the total MGRN1 protein levels remained unperturbed across samples. This may be extrapolated to suggest that increased proportion of cytosolic MGRN1 stabilizes Gα$_i$-GDP during interphase and elevates its steady-state levels. This is then efficiently recruited to the cell cortex during mitosis, where it helps in the assembly of the ternary complex.

Since all MGRN1 isoforms have *nes*, this motif should have an important role in governing the nuclear localisation of MGRN1. To validate the role of subcellular partitioning of MGRN1 in stabilisation of Gα$_i$, we generated mutants that either disrupted the *nes* (MGRN1ΔN150, MGRN1ΔN200*)* or had a mutated *nes* (MGRN11201D) (Fig. 5A).

Localisation of RFP tagged MGRN1 was altered in *nes* mutants (MGRN1ΔN200 and MGRN1I201D), where MGRN1 was observed in both the nucleus and the cytosol while in cells expressing MGRN1 with an intact *nes,* almost complete nuclear exclusion was seen (Fig. 5B). We checked for Gα$_i$ levels in whole cell lysates from MGRN1 mutants with or without a functional *nes*. In *nes* mutants, the protein levels of Gα$_i$ were less as compared to control cells with functional *nes* (Fig. 5C). Further, when cell lysates were fractionated to check for MGRN1 levels in the cytosolic and nuclear fractions, mutants which lacked a functional *nes* showed higher levels of MGRN1 in nuclear fractions compared to wild type or mutants with an intact *nes* motif (Fig. 5D-G). The ratio of MGRN1 in the nuclear versus cytosolic extracts tended towards 1 in cells transfected with MGRN1 *nes* mutants (MGRN1ΔN200 and MGRN1I201D) whereas in control cells the ratio was ~<0.4. However, the total MGRN1 protein levels remained unperturbed across samples. These results confirm that the partitioning of Gα$_i$ between the nucleus and cytosol affects the protein levels of Gα$_i$. Increase or decrease of Gα$_i$ levels from optimal levels may lead to mitotic anomalies in the *xy* plane. Alternately, it is also possible that MGRN1 regulates an intermediate molecule which then modulates the recruitment of Gα$_i$ at the membrane.

Taken together results so far elucidate that increased levels of Gα$_i$ promotes enhanced recruitment of the ternary complex at the membrane along with motor protein Dynein. This causes imbalance in the forces exerted on the spindle apparatus ultimately culminating in spindle defects observed in cells.

Negative regulation of Gα$_i$ reverses spindle defects generated by non-catalytic MGRN1

When Gα$_i$-YFP was overexpressed in cells, in combination with various MGRN1 constructs, significant lateral displacement was seen in cells expressing MGRN1-RFP versus its truncated mutants (Fig. 6A, B). The spindle displacement values obtained from cells co-transfected with Gα$_i$-YFP and MGRN1ΔR-RFP or MGRN1ΔC-RFP were ~1.4μ versus ~0.7μ in control samples. Since Gα$_i$ recruitment at the plasma membrane was elevated in the presence of MGRN1ΔR-RFP and MGRN1ΔC-RFP, we argued that myristoylation mutants of Gα$_i$-YFP should restore the lateral displacement phenotype observed in cells (since they cannot be recruited at the membrane). A rescue in lateral displacement was observed in cells co-transfected with Gα$_i$Δmyr-YFP and MGRN1ΔR-RFP or MGRN1ΔC-RFP (Fig. 6C). While a displacement of ≥1.1μ was observed in cells expressing full length MGRN1-RFP and Gα$_i$Δmyr-YFP, the amount of lateral displacement significantly reduced to ~0.7μ when cells

were transfected with MGRN1ΔR-RFP or MGRN1ΔC-RFP along with Gα$_i$Δmyr-YFP (Fig. 6D). This clearly indicates a reciprocal relationship between the recruitment of Gα$_i$ in the plasma membrane and the levels of cytosolic isoforms of MGRN1 in the cell.

DISCUSSION

This study establishes a unique and non-canonical function for the E3 ligase, MGRN1. We demonstratehow MGRN1, independent of its ligase activity, regulates the distribution of the ternary complex at the cell cortex and affects spindle positioning. Upon cellular fractionation, the cytosolic isoforms of MGRN1 are more abundant in the presence of MGRN1ΔR or MGRN1ΔC. This skews the protein distribution of Gα$_i$ and enriches it at the cortex than the poles. This is also reflected as an enrichment of a lower molecular weight monomeric Gα$_i$ form. It further leads to enrichment of the ternary complex at the plasma membrane, possibly regulating spindle positioning in the *xy* plane.

During interphase, LGN and Gα$_i$ are present in the cytosol while NuMa is localised to the nucleus. Post NEBD, during mitosis, Gα$_i$-LGN-NuMa complex is recruited to the plasma membrane in the cortical region by the myristoylation domain of Gα$_i$, and this recruitment occurs by the help of phosphatidylinositol (3,4,5)P3. Once at the cortex, NuMA/ LGN/Gα$_{i1–3}$, recruit Dynein to the cortex, which then directs spindle positioning by promoting pulling on astral microtubules (Gonczy 2008; Knoblich 2008; Kotak et al. 2013; Morin and Bellaıche 2011; Siller and Doe 2009).

Mice deficient in *Mgrn1* have developmental defects like congenital heart anomalies, abnormal craniofacial patterning and problems in the left-right (LR)-axis of symmetry. Though not embryonic lethal, there is an increased mortality rate during the weaning stages, suggesting that MGRN1 deficiency has a global effect at the organismal level. This study establishes novel function of MGRN1, independent of its ubiquitination activity, where the splice variants of the protein have a function different from the canonical ligase activity of the protein. This study, along with our previous report (Srivastava and Chakrabarti 2014) showing that MGRN1 stabilizes the MT polymerization, gives an insight into how MGRN1 affects spindle positioning, and thus development.

Alternative splicing of exon 12 and exon 17 produces four MGRN1 isoforms (Bagher et al. 2006; Jiao et al 2009). These MGRN1 isoforms have tissue specific expression patterns (Bagher et al. 2006), suggesting that the different MGRN1 isoforms have different physiologic functions and that loss of specific isoforms may underlie specific aspects of the MGRN1 null mutant phenotype.

Though suggested to be a cytoslic E3 ligase (Kim et al. 2007; Chakrabarti and Hegde 2009), reports also indicate a compartmentalization in the distribution of the various isoforms

of MGRN1 at the cellular level (Jiao et al. 2009). Studies from immunocytochemistry have shown that while isoform I and III are present in the cytosol, isoform II gets localized in the nucleus while isoform IV is predominantly present in the perinuclear region. Studies in transgenic mice indicate that while isoform I and III are able to compensate for *Mgrn1* null phenotype, isoform II is able to compensate for its loss only at very high expression levels whereas isoform IV fails to replace other isoforms in the skin or brain. This suggests distinct and unique functions that might be attributed to the different isoforms. A partial functional overlap between isoforms is also possible.

If the sub-cellular localization of the isoforms is altered, it can possibly lead to perturbation of MGRN1 function in the different sub-cellular compartments. Deletion of C-terminal in isoform II and IV leads to a loss of *nls* and concomitant enrichment of MGRN1 in the cytoplasm, where it could mimic isoform I. Further, it is possible that the deletion of RING domain leads to a change in the tertiary structure of the protein, affecting its ability to efficiently translocate to the nucleus. Our data shows an increase in the cortical localization of Gα$_i$ in the presence of MGRN1 mutants (MGRN1ΔR and MGRN1ΔC). A parallel increase in the protein levels of Gα$_i$ without perturbing its degradation suggests a ligase-independent function for MGRN1 whereby it can act as a chaperone to sequester monomeric Gα$_i$-GDP and stabilize it in the cytosol. This eventually gets reflected as higher amounts of Gα$_i$ at the cortex during mitosis, improper recruitment of the ternary complex along with Dynein and finally erroneous spindle positioning (Fig. 7). It is already established that ligases, like CHIP or STUB1 also have co-chaperone activity (Kampinga et al. 2003). Hence, a logical extension of this study would be to understand the role of MGRN1 in a similar capacity. However it cannot be undermined that since MGRN1 also modulates microtubule dynamics, alterations in the ternary complex might be due to a microtubule network alteration.

Acknowledgements: We are grateful to R. Mattera, S. Kotak and P. Gönczy for constructs, R. S. Hegde and C. Das for antibodies, and Rahul Kumar for generating MGRN1ΔC-RFP construct. P.K Chakraborty at Towa Optics (I) Pvt. Ltd. for help with microscopy experiments on the Nikon system. This work was supported by the "Integrative Biology on Omics Platform Project", intramural funding of the Department of Atomic Energy (DAE), Government of India.

Conflict of interest: The authors declare no conflict of interest, financial or otherwise.

REFERENCES

Bagher P, Jiao, J, Owen Smith, C, Cota, CD, Gunn, TM. 2006. Characterization of Mahogunin Ring Finger-1 expression in mice. Pigment Cell Res. **19**(6):635-43

Bird SL, Heald, R, Weis, K., 2013. RanGTP and CLASP1 cooperate to position the mitotic spindle. Mol Biol Cell. **24**(16):2506-14

Chakrabarti, O, Hegde, RS. 2009. Functional depletion of mahogunin by cytosolically exposed prion protein contributes to neurodegeneration. Cell **137**(6):1136-47

Chen CA, Manning, DR. 2001. Regulation of G proteins by covalent modification. Oncogene **20**(13):1643-52

Du Q, Macara IG. 2004. Mammalian Pins is a conformational switch that links NuMA to heterotrimeric G proteins. Cell **119**(4):503-16

Gillies TE, Cabernard C. 2011. Cell division orientation in animals. Curr Biol. **21**(15):R599-609

Gönczy, P. 2008. Mechanisms of asymmetric cell division: flies and worms pave the way. Nat. Rev Mol Cell Biol. **9**(5):355-66

Jiao J, Kim HY, Liu RR, Hogan CA, Sun K, Tam LM, Gunn TM. 2009. Transgenic analysis of the physiological functions of Mahogunin Ring Finger-1 isoforms. Genesis **47**(8):524-34

Kampinga HH, Kanon B, Salomons FA, Kabakov AE, Patterson C. 2003. Overexpression of the co chaperone CHIP enhances Hsp70-dependent folding activity in mammalian cells. Mol Cell Biol. **23**(14):4948-58

Kim BY, Olzmann JA, Barsh GS, Chin LS, Li L. 2007. Spongiform neurodegeneration-associated E3 ligase Mahogunin ubiquitylates TSG101 and regulates endosomal trafficking. Mol Biol Cell. **18**(4):1129-42

Kiyomitsu T, Cheeseman IM. 2012. Chromosome- and spindle-pole-derived signals generate an intrinsic code for spindle position and orientation. Nat Cell Biol. **14**(3):311-7

Knoblich JA. 2008. Mechanisms of Asymmetric Stem Cell Division. Cell **132**(4):583-97

Kotak S, Busso C, Gönczy P. 2012. Cortical dynein is critical for proper spindle positioning in human cells. J Cell Biol. **199**(1):97-110

Kotak S, Busso C, Gönczy P. 2013. NuMA phosphorylation by CDK1 couples mitotic progression with cortical dynein function. EMBO J. **32**(18):2517-29

Majumder P and Chakrabarti O. 2015. Mahogunin Regulates Fusion between Amphisomes/MVBS and Lysosomes via Ubiquitination of TSG101. Cell Death Dis. 6:e1970.

Matsumura S, Hamasaki M, Yamamoto T, Ebisuya M, Sato M, Nishida E, Toyoshima F. 2012. ABL1 regulates spindle orientation in adherent cells and mammalian skin. Nat Commun. 3:626

McNally, FJ. 2013. Mechanisms of spindle positioning. J. Cell Biol. **200**(2):131-40

Morin X, Bellaïche Y. 2011. Mitotic Spindle Orientation in Asymmetric and Symmetric Cell Divisions during Animal Development. Dev Cell. **21**(1):102-19

Pérez-Oliva AB, Olivares C, Jiménez-Cervantes C, García-Borrón JC. 2009. Mahogunin Ring Finger-1 (MGRN1) E3 Ubiquitin Ligase Inhibits Signaling from Melanocortin Receptor by Competition with Gs. J Biol Chem. **284**(46):31714-25

Siller KH, Doe CQ. 2009. Spindle orientation during asymmetric cell division. Nat. Cell Biol. **11**(4):365-74

Srivastava D, Chakrabarti O. 2014. Mahogunin-mediated α-tubulin ubiquitination via noncanonical K6 linkage regulates microtubule stability and mitotic spindle orientation. Cell Death Dis. 5:e1064

Srivastava D, Chakrabarti O. 2015. Ubiquitin in regulation of spindle apparatus and its positioning: implications in development and disease. Biochem Cell Biol. **93**(4):273-81

Stevermann L, Liakopoulos D. 2012. Molecular mechanisms in spindle positioning: structures and new concepts. Curr. Opin. Cell Biol. **24**(6):816-24

Woodard GE, Huang NN, Cho H, Miki T, Tall GG, Kehrl JH. 2010. Ric-8A and Gi alpha recruit LGN, NuMA, and Dynein to the cell cortex to help orient the mitotic spindle. Mol Cell Biol. **30**(14):3519-30

FIGURE LEGENDS

Figure 1: MGRN1 mutants cause defects in spindle positioning.

(A) Cartoon representation of ideal spindle positioning and various defects that occur in the *xy* plane or along the z axis.

(B) HeLa cells transiently expressing either MGRN1-RFP or MGRN1ΔR-RFP were immunostained for γ-tubulin and imaged. The channels for acquiring the images are indicated. Scale bar, 5μ.

(C) HeLa cells transiently expressing either MGRN1-RFP or MGRN1ΔR-RFP were immunostained for α-tubulin and imaged. The channels for acquiring the images are indicated. Scale bar, 5μ.

(D) Graph depicts the lateral displacement of spindle from the centre of the cells analysed in panel B and C. Note significant increase in lateral spindle displacement in the presence of MGRN1ΔR-RFP.* p≤0.01, using Student's t-test. Error bars + SEM.

(E) Graph representing the angular displacement calculated by analysis of cells from panel B and C. Cells transfected with MGRN1ΔR have angular displacement of ~25° while that for cells expressing MGRN1 is ~18°.** p≤0.001, using Student's t-test. Error bars + SEM.

(F) HeLa cells expressing MGRN1-RFP or MGRN1ΔC-RFP were immunostained for γ-tubulin and imaged. The channels for acquiring the images are indicated. Scale bar, 5μ.

(G) HeLa cells expressing MGRN1-RFP or MGRN1ΔC-RFP were immunostained for α-tubulin and imaged. The channels for acquiring the images are indicated. Scale bar, 5μ.

(H) Cells imaged in panel F and G were analysed to plot lateral displacement. Cells expressing MGRN1ΔC-RFP closely phenocopied the results of MGRN1ΔR-RFP, where again an increase in lateral displacement was detected when compared with the control (MGRN1). * p≤0.01, using Student's t-test. Error bars + SEM.

(I) Graph depicts the angular displacement calculated by analysis of cells from panel F and G. Note an increase in angular displacement in cells with MGRN1ΔC-RFP. * p≤0.01, using Student's t-test. Error bars + SEM.

Figure 2: MGRN1 alters the localization of Gα$_i$ in mitotic cells at the cortex.

(A) Schematic representation of Gα$_i$ protein expression during mitosis.

(B) Representative diagram showing the calculation of intensity along the axis of the spindle apparatus. To quantitate the variation in localization of Gα$_i$-YFP along the axis of division, a

straight line is drawn across the same and the intensity is plotted along each point of the line. A clear enrichment of the protein is seen at the membrane, as indicated by the two peaks in the representative plot.

(C) HeLa cells co-transfected with MGRN1-RFP or its truncated mutants along with Gα$_i$-YFP or empty vector control were synchronised and imaged. Gα$_i$-YFP was enriched at cortical region in cells transfected with MGRN1ΔR-RFP or MGRN1ΔC-RFP in greater amounts, against the controls. The channels for acquiring the images are indicated. Scale bar, 5μ.

(D) Variation in intensity of Gα$_i$ levels was calculated and plotted for cells transfected with MGRN1ΔR-RFP and compared with MGRN1-RFP cells. Note higher levels of Gα$_i$-YFP observed at the membrane in cells overexpressing MGRN1ΔR-RFP. Error bars + SEM.

(E) In a similar plot as panel D, the variation in the Gα$_i$ levels was calculated for cells transfected with MGRN1ΔC-RFP. For ease of comparison the same data as in panel D was used for the control cell. The levels of Gα$_i$-YFP at the cortex were similarly enhanced in the presence of MGRN1ΔC or MGRN1ΔR. Error bars + SEM.

Figure 3: Effect of MGRN1 and its mutants on the proteins of the ternary complex regulating spindle positioning.

(A) HeLa cells transfected with empty vector RFP, MGRN1-RFP or its truncated mutants (MGRN1ΔR-RFP, MGRN1ΔC-RFP and MGRN1ΔN-RFP) were synchronised, lysed and immunoblotted using indicated antibodies. While the levels of NuMa and Dynein were unaltered across samples, Gα$_i$ level was increased in the presence of MGRN1ΔR-RFP and MGRN1ΔC-RFP as against MGRN1-RFP or MGRN1ΔN-RFP. Similar pattern of expression was also seen in case of cells co-transfected with Gα$_i$-YFP with MGRN1-RFP or its truncated mutants. Immunoblots of Vinculin, GAPDH and MGRN1 serve as loading control.

(B) Histogram plotting the expression levels of Gα$_i$-YFP from lysates represented in panel A. An increase in the expression levels of Gα$_i$-YFP was observed in cells expressing MGRN1ΔR-RFP or MGRN1ΔC-RFP when compared with those expressing MGRN1-RFP or empty vector control.** $p \leq 0.001$,* $p \leq 0.01$, using Student's t-test. Error bars + SEM.

(C) HeLa cells co-transfected with MGRN1-RFP or its truncated mutants and Gα$_i$-YFP were mitotically synchronised and subjected to MG132 treatment. Similar pattern of expression of Gα$_i$-YFP was observed across samples, independent of presence or absence of MG132, indicating that Gα$_i$-YFP is not a substrate for proteasomal degradation by MGRN1. The

levels of β–tubulin serve as loading control. The levels of β–catenin protein were monitored to validate the efficiency proteasome blockade.

(D) HeLa cells transfected with HA-Ub, Gα$_i$-YFP and various MGRN1 constructs were subjected to *in vivo* ubiquitination assay. Lysates collected from these samples were subjected to immunoprecipitaton using anti-YFP antibody, followed by immunoblotting using anti-HA antibody. The absence of ubiquitination smear in the lanes (ii)-(iv) indicated that Gα$_i$ did not get ubiquitinated by MGRN1. (i) Validation of the efficiencies of HA-Ub and MGRN1 constructs in the ubiquitination of α-tubulin was noted by the presence of polyubiquitination smear in this lane. This lane represents HeLa lysate co-transfected with HA-Ub and MGRN1, followed by immunoprecipitation of α-tubulin. The status of ubiquitination was checked using anti-HA antibody. The blot was stripped and probed separately for Gα$_i$ or α-tubulin. ## denotes IgG heavy chain and ← indicates the Gα$_i$-YFP in (ii)-(iv). Similar molecular weights of α-tubulin and IgG heavy chain make distinguishing between the two difficult in lane (i). The levels of MGRN1 serve as loading control.

(E) Cartoon representation of the various isoforms of MGRN1.

(F) RNA was isolated from lysates collected from mitotically synchronised cells, transfected with Gα$_i$-YFP and the different MGRN1-RFP constructs or appropriate empty vector control. No significant variation in the transcript levels of Gα$_i$ was detected across samples analysed via quantitative RT-PCR.

Figure 4: Cytosolic forms MGRN1 stabilize monomeric Gα$_i$.

(A) Lysates from HeLa cells transfected with Gα$_i$-YFP along with MGRN1-RFP, MGRN1ΔR-RFP or MGRN1ΔC-RFP were resolved by native-PAGE and immunoblotted using anti-YFP antibody. Note abundance of monomeric Gα$_i$ in the presence of MGRN1ΔR and MGRN1ΔC, while more of the protein is in the trimeric G-protein complex in MGRN1-RFP expressing cells. The levels of MGRN1 and GADPH in the denatured samples serve as loading control.

(B) Representative plot showing the ratio of trimeric Gα$_i$-GTP to monomeric Gα$_i$-GDP observed on native immunoblots in cells expressing MGRN1-RFP, MGRN1ΔR-RFP or MGRN1ΔC-RFP. This ratio was higher in cells expressing MGRN1-RFP versus cells expressing MGRN1ΔR-RFP or MGRN1ΔC-RFP. Error bars + SEM.

(C) HeLa cells expressing MGRN1-RFP or its truncated mutants were lysed and subjected to fractionation studies. The cytoplasmic and nuclear fractions were analysed by immunoblotting for MGRN1. Under steady-state conditions in non-synchronised cells,

MGRN1 was detected primarily in the cytosol, while a small portion is also present in the nuclear fractions. A drastic reduction in MGRN1 levels in the nuclear fraction was seen in MGRN1ΔR samples, while in the presence of MGRN1ΔC, this amount was almost negligible. Note similar protein levels of MGRN1 prior to fractionation across samples. The efficiency of fractionation was validated by the levels of GAPDH and Histone H3.

(D) The ratio of MGRN1 protein levels in nuclear and cytosolic fractions was plotted from three independent fractionation experiments. Note a reduction in the nuclear versus cytosolic MGRN1 ratio in MGRN1ΔR and MGRN1ΔC samples. Error bars, ±standard deviation.

(E) The plot shows the distribution of MGRN1 in the nuclear (2X) and cytosol (1X) fractions in the various samples immunoblotted in panel C.

(F) The graph authenticates that GAPDH was detected in the cytosolic fractions and Histone H3 was seen only in the nuclear fractions.

Figure 5: Lack of functional *nes* alters Gα$_i$ protein levels and nuclear MGRN1: cytosolic MGRN1 ratio.

(A) Line diagram showing MGRN1 and its *nes* mutants.

(B) HeLa cells transiently transfected with the various RFP tagged MGRN1 constructs as indicated in the figure were imaged 24 hours post-transfection to verify their expression and localisation microscopically. Note abundance of nuclear MGRN1 in cells expressing MGRN1ΔN200-RFP and MGRN1I201D-RFP.

(C) HeLa cells transfected with MGRN1-RFP or its mutants (MGRN1ΔN150-RFP, MGRN1ΔN200-RFP and MGRN1I201D-RFP) were synchronised, lysed and immunoblotted using indicated antibodies. Gα$_i$ levels decreased in the presence of MGRN1ΔN200-RFP and MGRN1I201D-RFP as against MGRN1-RFP. Similar pattern of expression was also seen in case of cells co-transfected with Gα$_i$-YFP with MGRN1-RFP or its mutants. Immunoblots of GAPDH and MGRN1 serve as loading control.

(D) HeLa cells expressing MGRN1-RFP or its *nes* mutants were lysed and subjected to fractionation studies similar to panel 4C. The cytoplasmic and nuclear fractions were analysed by immunoblotting for MGRN1. An increase in MGRN1 levels in the nuclear fraction was seen in MGRN1ΔN200 and MGRN1I201D samples, compared to MGRN1-RFP lysates. Note similar protein levels of MGRN1 prior to fractionation across samples. The efficiency of fractionation was validated by the levels of GAPDH and Histone H3.

(E) The ratio of MGRN1 protein levels in nuclear and cytosolic fractions was plotted from three independent fractionation experiments. Error bars, ± standard deviation.

(F) The plot shows the distribution of MGRN1 in the nuclear (2X) and cytosol (1X) fractions in the various samples immunoblotted in panel D.

(G) The graph authenticates that GAPDH was detected in the cytosolic fractions and Histone H3 was seen only in the nuclear fractions.

Figure 6: Gα$_i$Δmyr reverses the spindle positioning defects induced by functional mutants of MGRN1.

(A) HeLa cells were co-transfected with Gα$_i$-YFP and MGRN1-RFP or its truncated mutants and imaged. The channels for acquiring the images are indicated. Scale bar, 5μ.

(B) Histogram analysis of the lateral displacement of the spindle apparatus in cells imaged for analysis in panel A. Note a significantly increased lateral displacement of the mitotic spindle in cells expressing truncated mutants of MGRN1 in comparison with MGRN1. *** $p \leq 0.0001$,* $p \leq 0.01$, using Student's t-test. Error bars + SEM.

(C) Cells were co-transfected with Gα$_i$Δmyr-YFP and various MGRN1 constructs and imaged. The channels for acquiring the images are indicated. Scale bar, 5μ.

(D) Histogram analysis of the lateral displacement of the spindle apparatus in cells from samples in panel C. Note a significant reduction in this displacement in cells with MGRN1ΔR or MGRN1ΔC and Gα$_i$Δmyr versus MGRN1.*** $p \leq 0.0001$, using Student's t-test. Error bars + SEM.

Figure 7: MGRN1 regulates Gαi localisation during mitosis and spindle positioning. Cartoon representation summarising the role of MGRN1 in regulating the spindle apparatus position during mitosis. Under normal conditions, cytosolic isoforms of MGRN1 facilitate the stabilization and recruitment of Gα$_i$ at the membrane. An imbalance in the concentration of cytosolic isoforms of MGRN1 leads to enrichment of Gα$_i$ at the membrane and spindle positioning defects.

SUPPLEMENTAL FIGURE LEGENDS

Figure S1: MGRN1 mutants cause defects in spindle tilt.

(A) HeLa cells exogenously expressing MGRN1-RFP, MGRN1ΔR-RFP or MGRN1ΔC-RFP was immunostained for α-tubulin and imaged. The channels for acquiring the images are indicated.

(B) Plot representing the distribution of spindle tilt in cells expressing MGRN1ΔR-RFP versus cells expressing fully functional MGRN1-RFP. While cells expressing MGRN1 (represented in blue) showed a minimal tilt of ≤ 10°, those with MGRN1ΔR had a spindle tilt of ≥ 20° for a major percentage of cells (~40%).

(C) Plot depicts the distribution of spindle tilt in cells expressing MGRN1ΔC-RFP versus cells expressing fully functional MGRN1-RFP. While cells expressing MGRN1 (represented in blue) showed a minimal tilt of ≤ 10°, cells expressing MGRN1ΔC showed a spindle tilt of ≥ 30° for a major percentage of cells (~70%). It is noteworthy that the tilt observed in this case is higher than cells expressing MGRN1ΔR.

(D) HeLa cells transiently transfected with the various MGRN1 constructs as indicated in the figure were imaged 24 hours post-transfection to verify their expression microscopically. These cells were then lysed and immunoblotted with anti-RFP antibody to verify the expression of the constructs biochemically. The cartoon representation indicates the regions deleted in full length MGRN1 to design the various truncated mutants of MGRN1.

(E) HeLa cells co-transfected with HA-Ub, and MGRN1-RFP or its truncated mutants, MGRN1ΔR-RFP or MGRN1ΔC-RFP, were subjected to *in vivo* ubiquitination assay. Lysates collected from these samples were subjected to immunoprecipitaton using anti- α-tubulin antibody, followed by immunoblotting using anti-HA antibody. While ubiquitination of α-tubulin occurs in the presence of fully functional MGRN1, the presence of MGRN1ΔR or MGRN1ΔC adversely affects the ubiquitination of MGRN1 indicating that these domains are essential for ubiquitination of α-tubulin by MGRN1.

Figure S2:MGRN1 alters the localization of ternary complex proteins in mitotic cells at the cortex.

(A) Schematic representation of Dynein/NuMa protein expressions during mitosis.

(B) Cartoon depicting the distribution of these proteins in mitotic cells. To quantitate the variation in localization of a particular protein along the axis of division, a straight line is drawn across the cell and the intensity is plotted along each point of the line.

(C) HeLa cells overexpressing either MGRN1-RFP or MGRN1ΔR-RFP were immunostained for Dynein and imaged. The channels for acquiring the images are indicated.

(D) The variation in intensity of Dynein along the long axis of the cell was calculated and plotted for cells transfected with MGRN1ΔR-RFP as against those with MGRN1-RFP.

(E) Histogram plotting the ratio of the intensity of Dynein at the cortical region of the cell versus that at the spindle poles. Note that this ratio was ~2 folds more in cells expressing MGRN1ΔR-RFP when compared with those expressing MGRN1-RFP. *** p≤0.0001, using Student's t-test. Error bars + SEM.

(F) HeLa cells overexpressing either MGRN1-RFP or MGRN1ΔR-RFP were immunostained for NuMa and imaged. The channels for acquiring the images are indicated.

(G) The variation in intensity of NuMa was calculated as in panel D and plotted for cells transfected with MGRN1ΔR-RFP and compared with those expressing MGRN1-RFP.

(H) Histogram plotting the ratio of the intensity of NuMa at the cortical region of the cell versus that at the spindle poles. Note that this ratio was ~1.4 in cells expressing MGRN1ΔR while in those with MGRN1-RFP, this ratio was ~1. *** p≤0.0001, using Student's t-test. Error bars + SEM.

Figure S3: Effect of MGRN1 and its truncated mutants on Gα$_i$ is phenocopied in the presence of Gα$_i$Δmyr, while its point mutants do not affect Gα$_i$ levels.

(A) HeLa cells were co-transfected with myristoylation and palmitoylation mutant of Gα$_i$-YFP (Gα$_i$Δmyr–YFP) and MGRN1-RFP or truncated mutants (MGRN1ΔR-RFP or MGRN1ΔC-RFP). Lysates from mitotically enriched cells showed increase in expression levels of Gα$_i$-YFP in cells transfected with MGRN1ΔR or MGRN1ΔC as seen in Figure 3. The levels of GAPDH and MGRN1 serve as loading control.

(B) Histogram plotting the expression levels of Gα$_i$-YFP from lysates represented in panel A. An increase in the expression levels of Gα$_i$-YFP was observed in cells expressing MGRN1ΔR-RFP or MGRN1ΔC-RFP when compared with those expressing MGRN1-RFP. Error bars + SEM.

(C) HeLa cells were co-transfected with Gα$_i$–YFP and MGRN1-GFP or its point mutants (C316D MGRN1-GFP or SRAP MGRN1-GFP). Lysates collected from mitotically enriched cells showed no increase in expression levels of Gα$_i$-YFP unlike panel A.

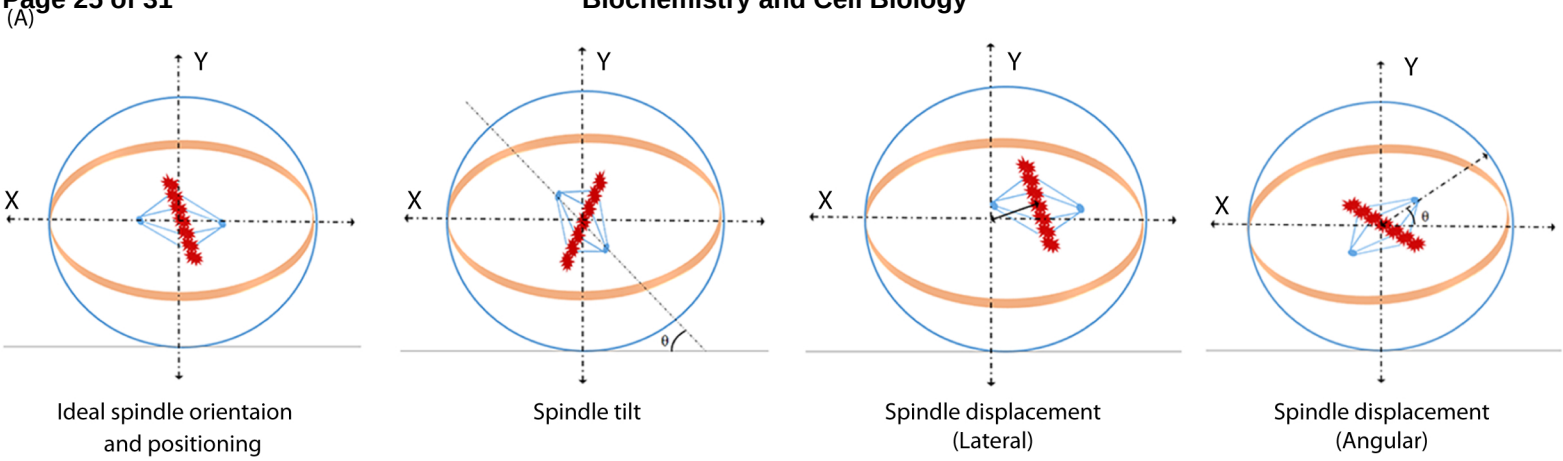

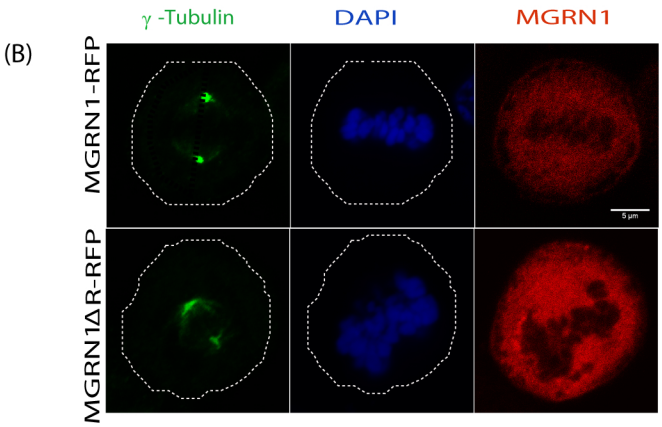

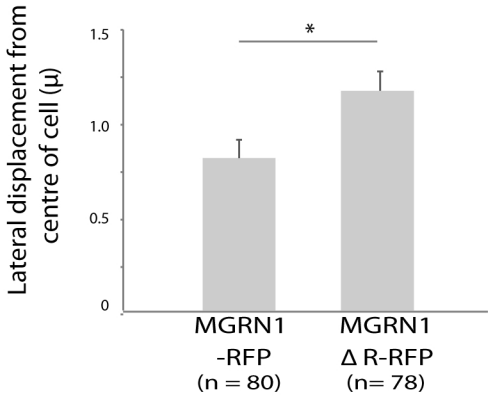

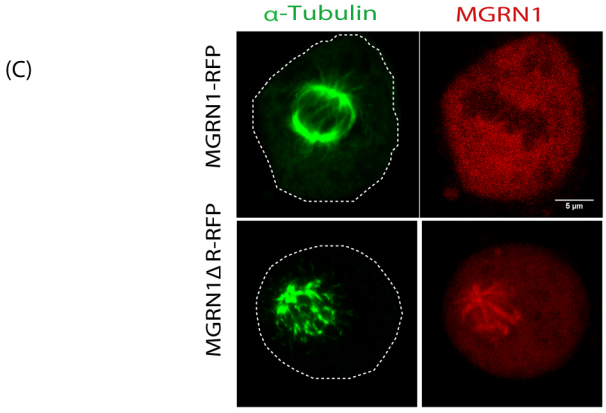

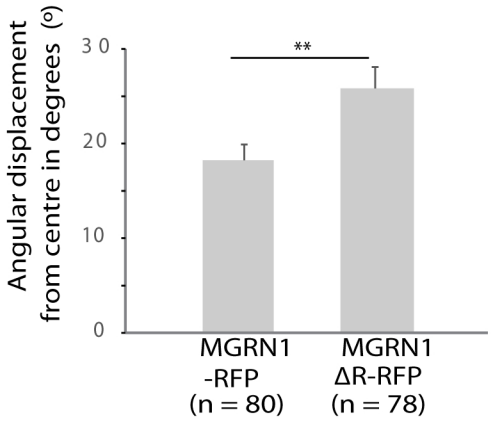

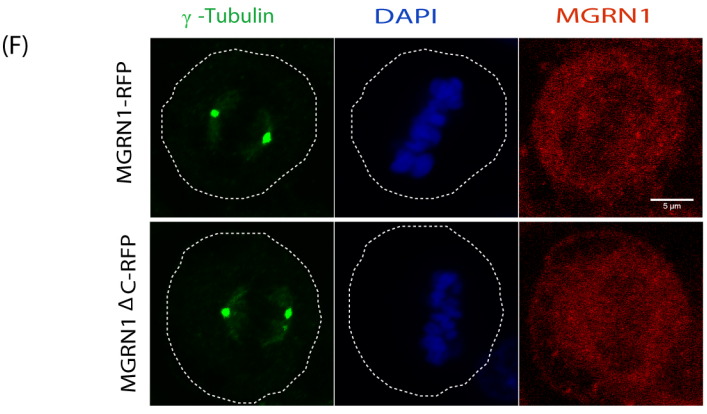

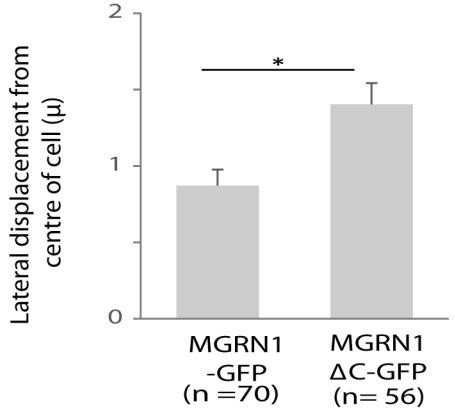

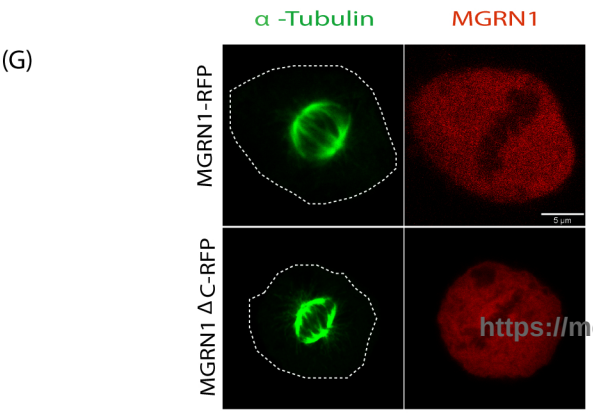

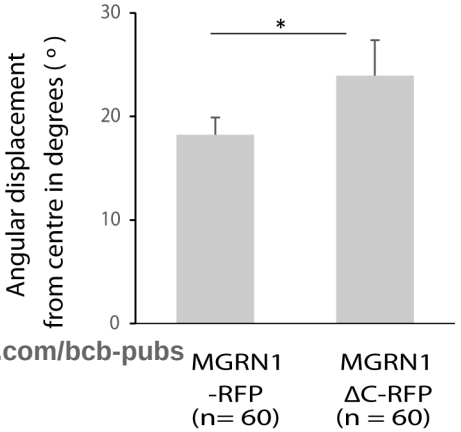

Figure 2

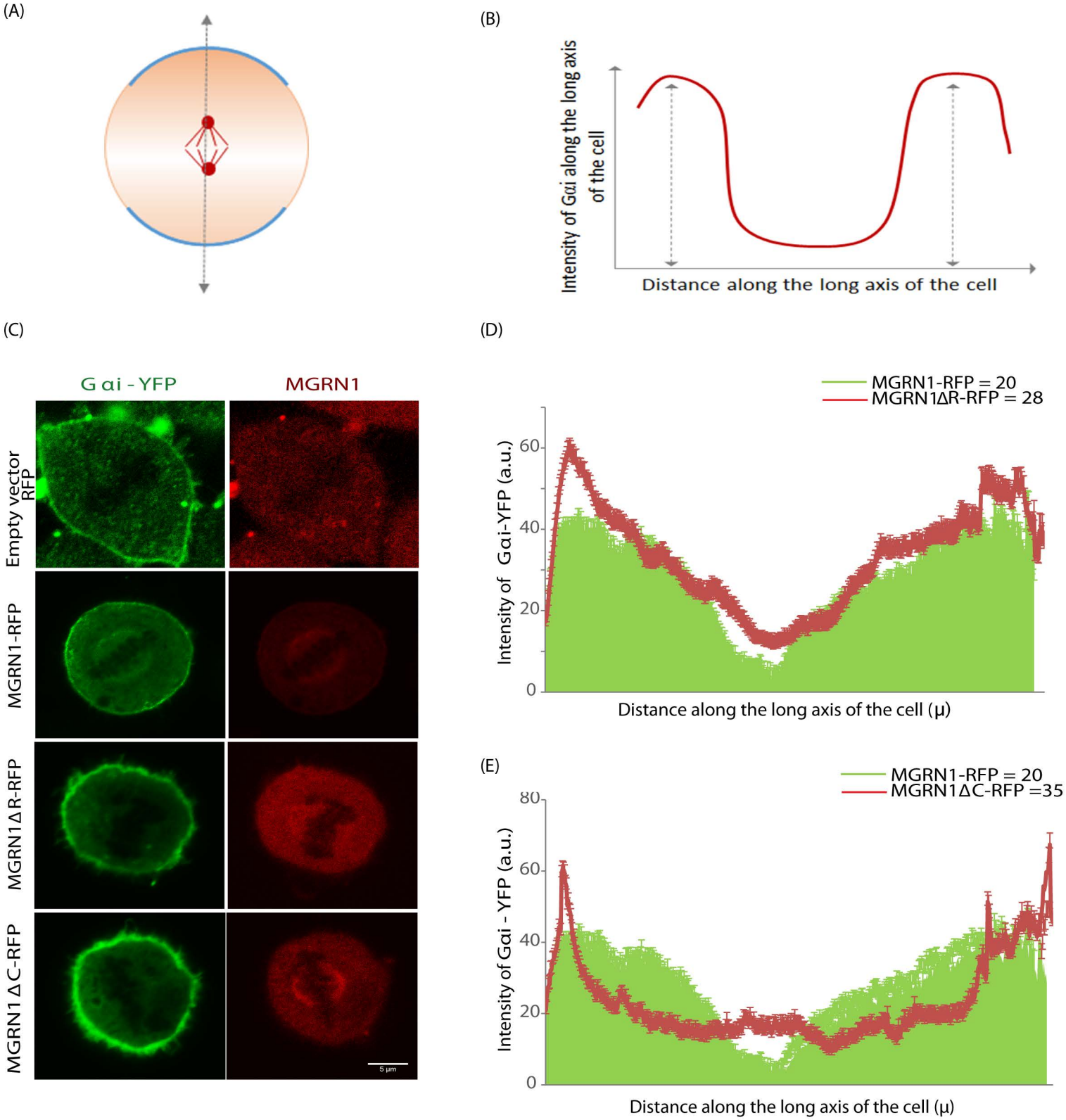
(A)
(B)
Intensity of Gαi along the long axis of the cell
Distance along the long axis of the cell
(C)
G αi - YFP
MGRN1
Empty vector RFP
MGRN1-RFP
MGRN1ΔR-RFP
MGRN1ΔC-RFP
5 µm
(D)
MGRN1-RFP = 20
MGRN1ΔR-RFP = 28
Intensity of Gαi-YFP (a.u.)
0
20
40
60
Distance along the long axis of the cell (µ)
(E)
MGRN1-RFP = 20
MGRN1ΔC-RFP =35
Intensity of Gαi - YFP (a.u.)
0
20
40
60
80
Distance along the long axis of the cell (µ)

Figure 3

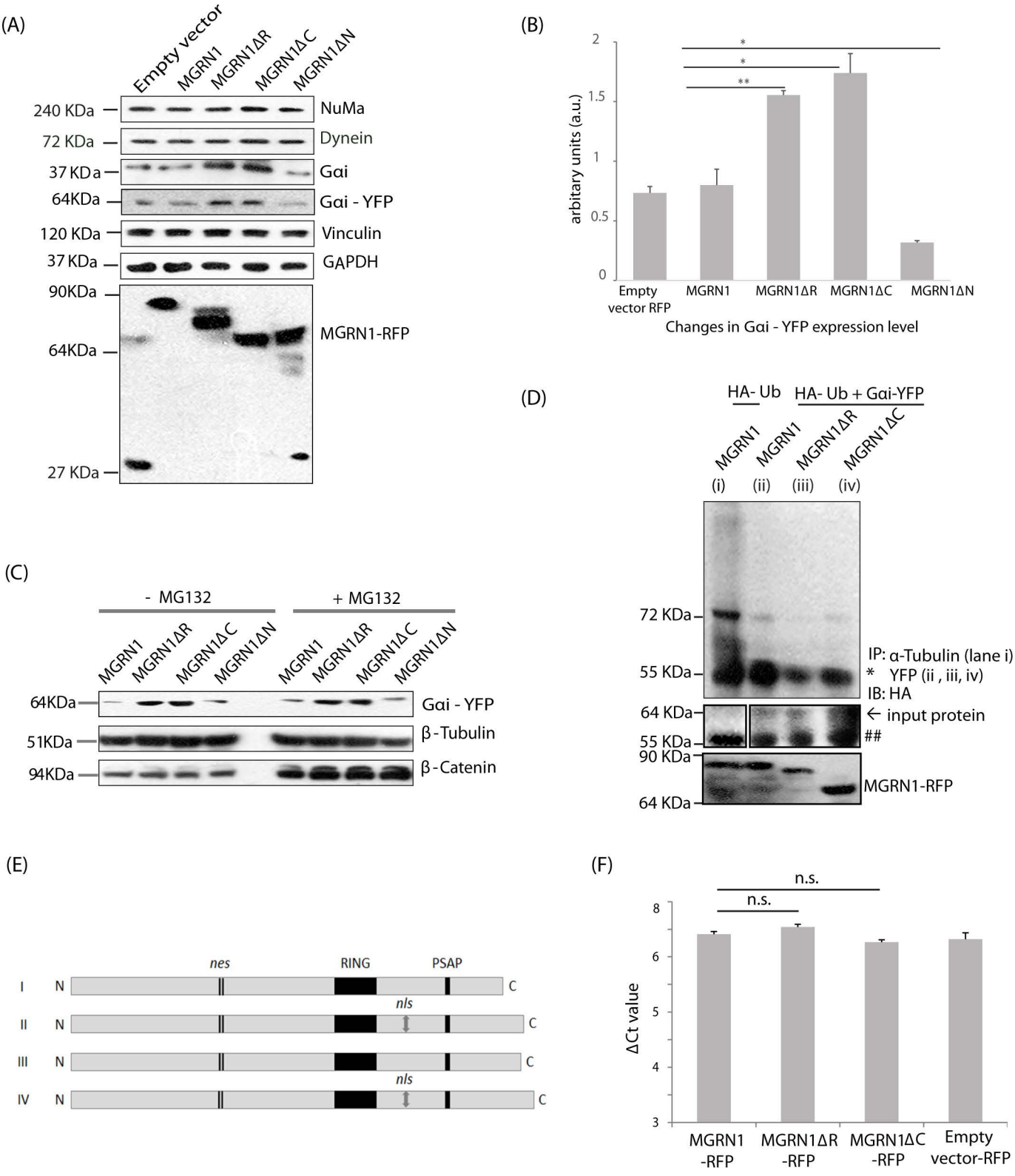
(A)
Empty vector
MGRN1
MGRN1ΔR
MGRN1ΔC
MGRN1ΔN
240 KDa
NuMa
72 KDa
Dynein
37 KDa
Gαi
64KDa
Gαi - YFP
120 KDa
Vinculin
37 KDa
GAPDH
90KDa
64KDa
27 KDa
MGRN1-RFP
(B)
arbitary units (a.u.)
2
1.5
1
0.5
0
*
*
**
Empty vector RFP
MGRN1
MGRN1ΔR
MGRN1ΔC
MGRN1ΔN
Changes in Gαi - YFP expression level
(C)
- MG132
+ MG132
MGRN1
MGRN1ΔR
MGRN1ΔC
MGRN1ΔN
64KDa
Gαi - YFP
51KDa
β-Tubulin
94KDa
β-Catenin
(D)
HA- Ub
HA- Ub + Gαi-YFP
MGRN1
MGRN1
MGRN1ΔR
MGRN1ΔC
(i)
(ii)
(iii)
(iv)
72 KDa
55 KDa
IP: α-Tubulin (lane i)
* YFP (ii , iii, iv)
IB: HA
64 KDa
← input protein
55 KDa
##
90 KDa
64 KDa
MGRN1-RFP
(E)
nes
RING
PSAP
I N C
nls
II N C
III N C
nls
IV N C
(F)
n.s.
n.s.
ΔCt value
8
6
5
4
3
MGRN1 -RFP
MGRN1ΔR -RFP
MGRN1ΔC -RFP
Empty vector-RFP

Figure 4

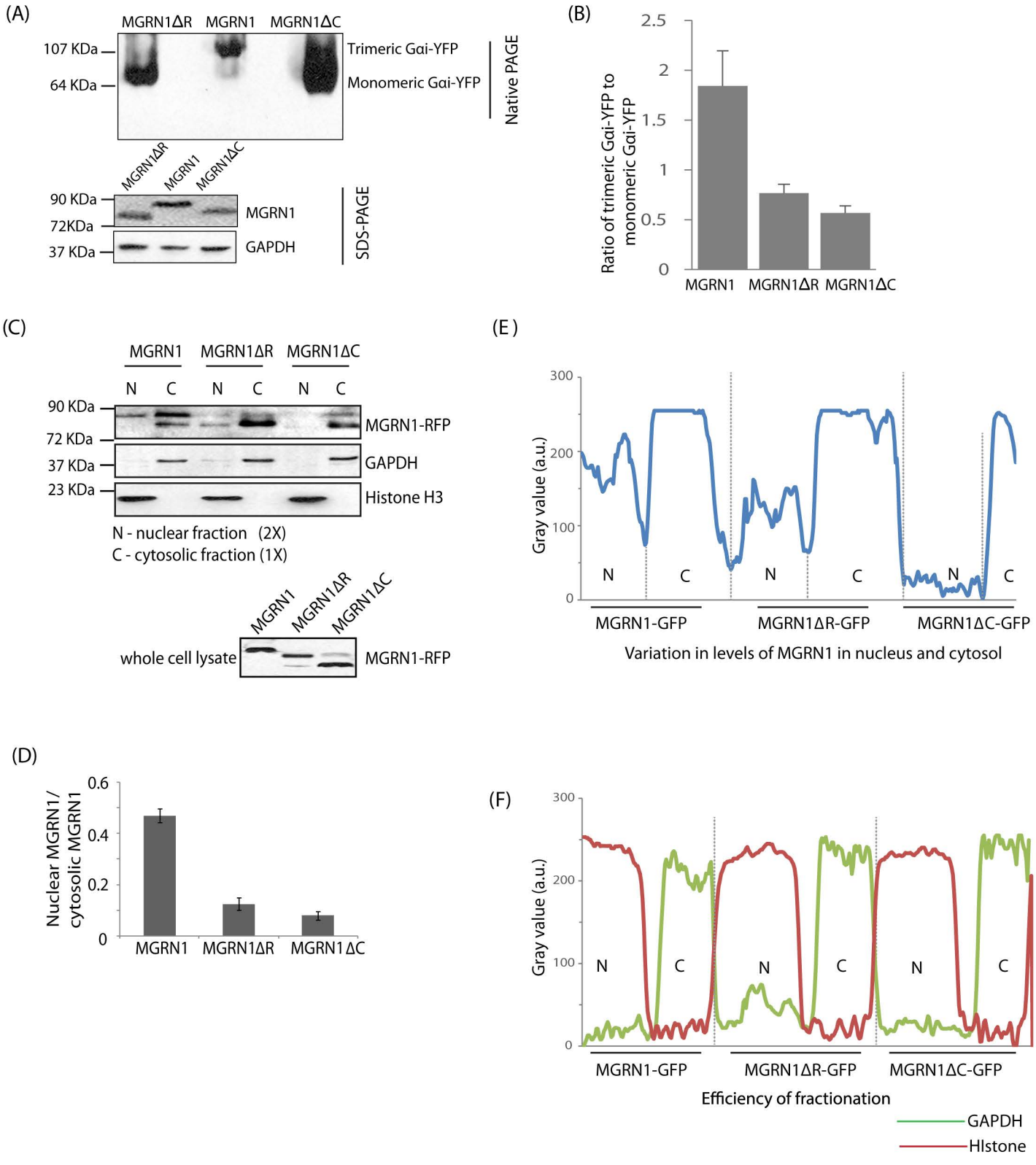
(A)
MGRN1ΔR MGRN1 MGRN1ΔC
107 KDa
64 KDa
Trimeric Gαi-YFP
Monomeric Gαi-YFP
Native PAGE
MGRN1ΔR MGRN1 MGRN1ΔC
90 KDa
72KDa
37 KDa
MGRN1
GAPDH
SDS-PAGE
(B)
Ratio of trimeric Gαi-YFP to monomeric Gαi-YFP
2.5
2
1.5
1
0.5
0
MGRN1 MGRN1ΔR MGRN1ΔC
(C)
MGRN1 MGRN1ΔR MGRN1ΔC
N C N C N C
90 KDa
72 KDa
37 KDa
23 KDa
MGRN1-RFP
GAPDH
Histone H3
N - nuclear fraction (2X)
C - cytosolic fraction (1X)
MGRN1 MGRN1ΔR MGRN1ΔC
whole cell lysate
MGRN1-RFP
(E)
Gray value (a.u.)
300
200
100
0
N C N C N C
MGRN1-GFP
MGRN1ΔR-GFP
MGRN1ΔC-GFP
Variation in levels of MGRN1 in nucleus and cytosol
(D)
Nuclear MGRN1/ cytosolic MGRN1
0.6
0.4
0.2
0
MGRN1 MGRN1ΔR MGRN1 ΔC
(F)
Gray value (a.u.)
300
200
100
0
N C N C N C
MGRN1-GFP
MGRN1ΔR-GFP
MGRN1ΔC-GFP
Efficiency of fractionation
GAPDH
Hlstone

Figure 5

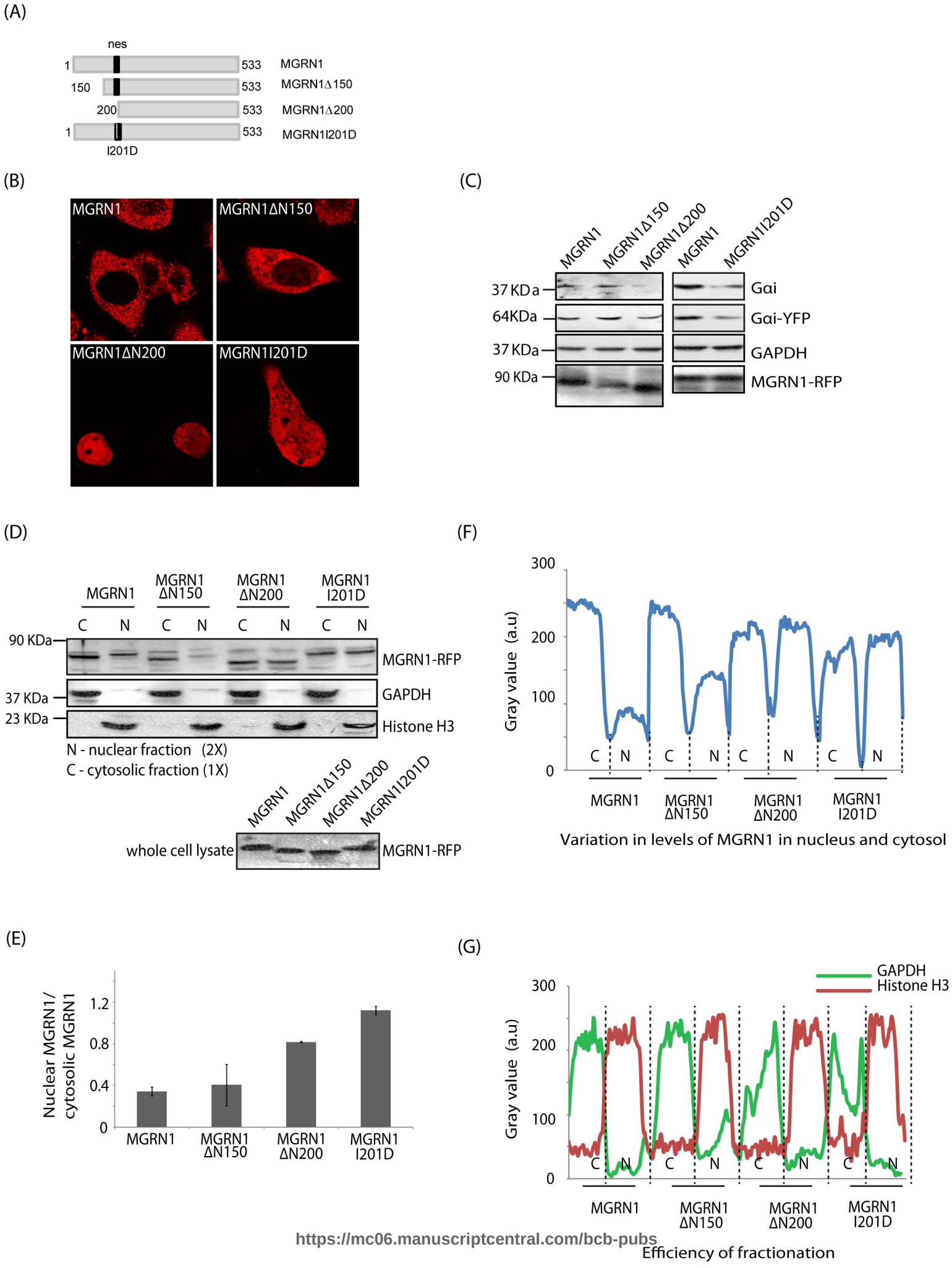
(A)
nes
1
533
MGRN1
150
533
MGRN1Δ150
200
533
MGRN1Δ200
1
533
MGRN1I201D
I201D
(B)
MGRN1
MGRN1ΔN150
MGRN1ΔN200
MGRN1I201D
(C)
MGRN1
MGRN1Δ150
MGRN1Δ200
MGRN1
MGRN1I201D
37 KDa
Gαi
64KDa
Gαi-YFP
37 KDa
GAPDH
90 KDa
MGRN1-RFP
(D)
MGRN1
MGRN1 ΔN150
MGRN1 ΔN200
MGRN1 I201D
C N C N C N C N
90 KDa
MGRN1-RFP
37 KDa
GAPDH
23 KDa
Histone H3
N - nuclear fraction (2X)
C - cytosolic fraction (1X)
MGRN1
MGRN1Δ150
MGRN1Δ200
MGRN1I201D
whole cell lysate
MGRN1-RFP
(F)
Gray value (a.u)
300
200
100
0
C N C N C N C N
MGRN1
MGRN1 ΔN150
MGRN1 ΔN200
MGRN1 I201D
Variation in levels of MGRN1 in nucleus and cytosol
(E)
Nuclear MGRN1/ cytosolic MGRN1
1.2
0.8
0.4
0
MGRN1
MGRN1 ΔN150
MGRN1 ΔN200
MGRN1 I201D
(G)
GAPDH
Histone H3
Gray value (a.u)
300
200
100
0
C N C N C N C N
MGRN1
MGRN1 ΔN150
MGRN1 ΔN200
MGRN1 I201D
Efficiency of fractionation

Figure 6

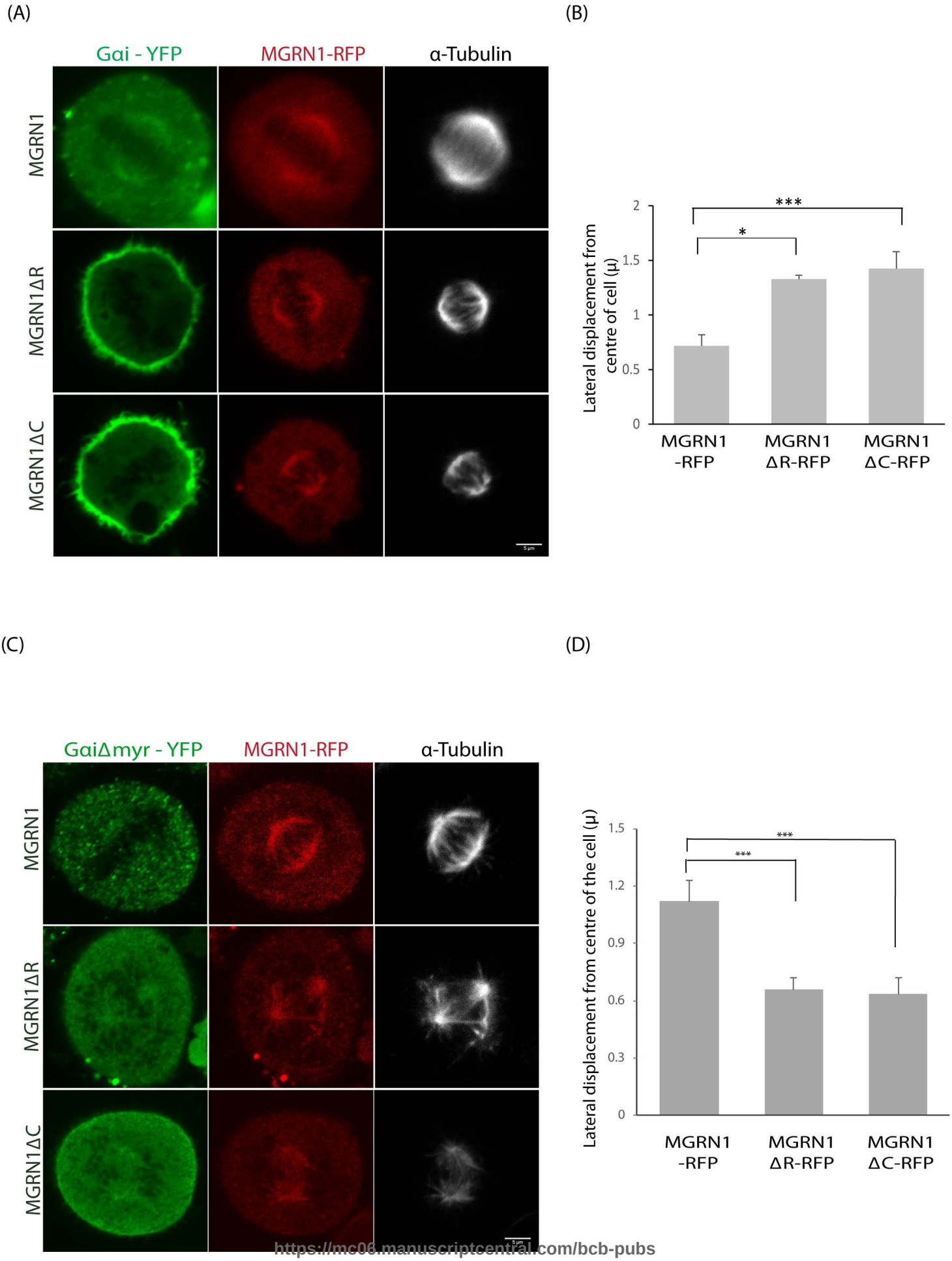

Figure 7

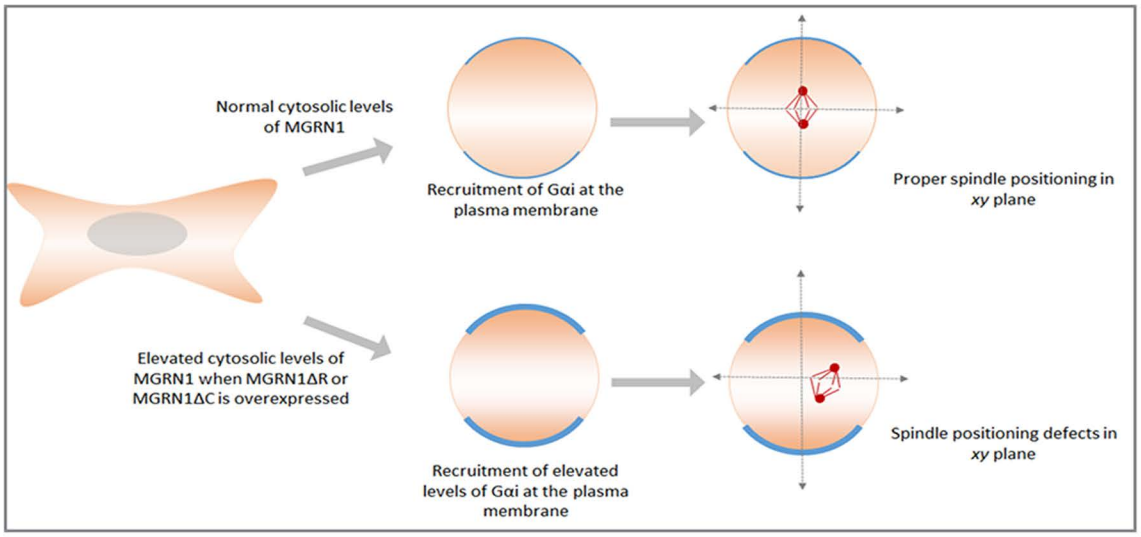
Normal cytosolic levels of MGRN1
Recruitment of Gαi at the plasma membrane
Proper spindle positioning in xy plane
Elevated cytosolic levels of MGRN1 when MGRN1ΔR or MGRN1ΔC is overexpressed
Recruitment of elevated levels of Gαi at the plasma membrane
Spindle positioning defects in xy plane